Synthesis of Gold Nanoparticles using the Interface of an Emulsion Droplet

Suchanuch Sachdev[1], Rhushabh Maugi[1], Jack Woolley[1], Caroline Kirk[2], Zhaoxia Zhou[3], Steven D. R. Christie[1], Mark Platt[1*]

1 - Department of Chemistry, Loughborough University, Loughborough, LE11 3TU. United Kingdom.
2- School of Chemistry, University of Edinburgh, David Brewster Road. Edinburgh, EH9 3FJ. United Kingdom.
3 - Loughborough Materials Characterisation Centre, Department of Materials, Loughborough University, Loughborough, LE11 3TU. United Kingdom.

* Email: m.platt@lboro.ac.uk; Tel: +441509 222 573

Abstract

A facile and rapid method for synthesising single crystal gold spherical or platelet (non-spherical) particles is reported. The reaction takes place at the interface of two immiscible liquids where the reducing agent decamethylferrocene (DmFc) was initially added to hexane, and gold chloride ($AuCl_4^-$) to an aqueous phase. The reaction is spontaneous at room temperature, leading to the creation of Au nanoparticles, (AuNP). A flow focusing microfluidic chip was used to create emulsion droplets allowing the same reaction take place within a series of microreactors. The technique allows the number of droplets, their diameter and even the concentration of reactants in both phases to be controlled. The size and shape of the AuNP is dependent upon the concentration of the reactants and the size of the droplets. By tuning the reaction parameters the synthesised nanoparticles vary from nanometre to micron sized spheres or platelets. The surfactant used to stabilise the emulsion was also shown to influence the particle shape. Finally, the addition of other nanoparticles within the droplet allows for core@shell particles to be readily formed, and we believe this could be a versatile platform for the large scale production of core@shell particles.

Key words: Microfluidic, Emulsion, core@shell, Nanosheets, Nanoparticles

Introduction

Synthetic methods for nanoparticle production have evolved to the extent that particle size, shape, and composition can be tuned[1–4]. They have been integrated into many aspects of modern life[5–10] such as information technology, medical equipment and energy. Gold nanoparticles (AuNPs) of varying morphologies are especially sought after as they have many applications in catalysis[11–13], biosensing[14–18] and therapeutics[19,20]. Anisotropic particles, in particular gold nanosheets and core@shell particles have gained particular attention[21–27] as they possess enhanced optical properties for the treatment of tumours[20], enhanced Raman detection[28] and optical sensors[29,30].

Synthetic strategies leading to highly anisotropic particles can require high temperatures, templates or polymer and molecular capping agents[31], however, there is an emerging trend to seek "green" chemistries for their production[19,20,32,33]. Continuous microfluidic flow reactors are a powerful tool for synthesizing materials[34]. The translation of batch chemistries onto continuous flow platforms represents an area of increased research as they offer reduced production costs, controlled and reproducible reaction parameters and scalable synthesis strategies[35,36]. A common strategy for synthesising nanomaterials within these reactors is to use emulsion droplets. Such systems have been used to create a range of materials including particles of high aspect ratios. Experimental variables explored for these systems include surfactants, solvents and droplets sizes. These have all been found to influence the products. An extensive review on the subject is covered elsewhere[37] and have been extensively applied to the production of AuNPs[38].

Other techniques for AuNP synthesis include single and two phase liquid-liquid (liq-liq) systems[39–43]. The interface between two immiscible liquids offers a defect free, reproducible substrate to grow and assemble metals[42,44]. This interface allows the material to be easily recovered, as the majority of the newly created particles remain at the interface upon creation[45]. The assembly of nanomaterials at the liq-liq interface is spontaneous due to the favourable stabilisation of the interfacial free energy and was first discovered by Ramsden[46] and Pickering[47].

The interface between two immiscible electrolyte solutions (ITIES) combines the defect free liq-liq interface, with the benefits of electrochemical strategies, allowing a degree of control over the growth and assembly of the material through the applied potential or template [40,43,48–58]. Alternative chemical based strategies for liq-liq reactions are also reported [45,52,58], such reactions place a reducing agent in one phase (e.g. organic) and a metal precursor in the second phase (e.g. aqueous) as shown in (Figure 1Di) and a wide range of synthetic strategies at these interfaces have been reported[37,38,59,60].

In this paper we present a strategy for producing Au nanomaterials, and Au@Fe_3O_4 particles using a simple chemical reaction at the interface of an emulsion droplet. Each droplet acts as a microreactor, and the size and shape of the nanoparticle (NP) is then determined by the concentration of the reactants, surfactant and the concentration of the droplets. By tuning the reaction parameters, either spherical single crystal AuNPs, single crystal micron sized Au platelets are produced. In contrast, the same reaction at a large free standing interface produces only spherical AuNPs. Finally we show how in the presence of a second pre-formed Fe_3O_4 nanoparticle (NP1) in the organic phase (Figure 1), we create

$Au@Fe_3O_4$ particles. We believe this could be a versatile platform for the large scale production of core@shell particles, and could be transferred to other metals in future.

Materials and methods

Chemicals and reagents

The following chemicals were purchased from Sigma Aldrich, U.K. and unless stated the chemicals were used without purification. Sodium Dodecyl Sulfate (SDS) (436143), Iron (ll) chloride tetrahydrate ($FeCl_2 \cdot 4H_2O$) (220299), Iron (lll) chloride hexahydrate ($FeCl_3 \cdot 6H_2O$) (236489), ammonium hydroxide ($NH_3 \cdot H_2O$) (338818), Oleic acid (364525), perchloric acid (244252), Gold (lll) chloride trihydrate (≥ 49%) (G4022), Tetraoctylammonium bromide (98%) (294136), 12-mercaptododecanoic acid (12-MDA) (675067), Bis(pentamethylcyclopentadienyl) iron (ll) (97%, 378542), sodium borohydride (98%) (452882). The following chemicals were purchased from VWR chemicals, U.K. Hexane (24580.324), ethanol absolute (20821.330), toluene (28676.322), were used. Deionized (DI) water with a resistivity of 18.2 MΩcm was used throughout.

A 14 μm etch depth Dolomite hydrophilic x-junction "small droplet chip" (Part No. 3200136), Dolomite Mitos P-Pump basic (Part No. 3200175) were controlled via the Dolomite Mitos Flow Control Centre Version 2.2.15. The small droplet chip was made from glass and can generate droplets with a diameter of 5-30 μm. The surface of the channel is hydrophilic to produced oil-in-water droplets.

Synthesis of hydrophobic nanomagnetic particles (250 mL) scale

$FeCl_2 \cdot 4H_2O$ (12 g) and $FeCl_3 \cdot 6H_2O$ (24.5 g) were dissolved in DI-water (62.5 mL) in a 250 mL three-neck round bottom flask. The flask was placed in an ice bath. $NH_3 \cdot H_2O$ (50 mL) was added rapidly with vigorous stirring. The flask was left in the ice bath for 45 minutes. The solution was rapidly heated to 85^{o}C for 1 hour. Oleic acid (7.5 mL) was then added and the solution was further heated for another 1 hour. The flask was cooled to room temperature and the black precipitate was transferred to a 150 mL beaker. The black precipitate was washed 3 times with ethanol (50 mL) and each time the black magnetite was collected using a block magnet. The black precipitate was then washed 3 times with DI-water (50 mL) before washing 3 times with 20% perchloric acid (50 mL) to dissolve $Fe(OH)_2$ and $Fe(OH)_3$. The black precipitate was again washed 3 times with DI-water (50 mL), followed by three times wash with ethanol (50 mL). Hexane (87.5 mL) was added to the resultant particles to aid dispersion, this was called ferrofluid. Ferrofluid (1mL) was taken into an Eppendorf tube and allowed it to evaporate overnight. The particle concentration was determined by weighing the mass of the material that remained after evaporation.[61]

Synthesis of gold nanoparticles coated with 12-mercaptododecanoic acid in toluene.

Gold nanoparticles were prepared by a previously reported technique[40], briefly $HAuCl_4$ (0.05 M, 4 mL) was mixed with tetraoctylammonium bromide in toluene (0.05 M, 11 mL) in a vial. The mixture was left stirring for a minimum of 2 h. The organic phase was then transferred to another vial and 12-mercaptododecanoic acid (1200 μL) was added followed by the addition of freshly prepared $NaBH_4$ (0.4 M, 25 mL) with vigorous stirring. Colour change from orange to deep brown indicated the reactions completion. The mixture was left stirring for a

minimum of 3 h. The organic phase was separated from the mixture and transferred to a clean vial. The organic phase (500 µL) of the Au-NP solution was transferred to an Eppendorf tube allowing the solvent to be evaporated to dryness. Ethanol (1500 µL) was then added to the precipitate in the Eppendorf, followed by 2 drops of NaOH (5 M). The Eppendorf was vortexed to disperse the pellet and then kept in the freezer for 16 h following centrifugation at 12000 rpm for 5 min. The supernatant was removed and washed twice with ethanol (1000 µL) followed by DI-water (100 µL). At this point the particles had dispersed into the aqueous solution and it appeared brown.

Creation of emulsion droplets

Hexane, (P1) and aqueous solution (P2) were connected to the droplet chip as shown in figure 1. P2 was the continuous phase and the droplets size of P1 was controlled by varying the flow rates of P1:P2. The droplet size was observed through a Celestron LCD digital microscope Model ~44340 and measured by analyzing an image taken on the microscope as shown in Figure 1. The droplets were collected in the collection/ reaction pot (10 mL glass vial) and left open to the atmosphere for 2-3 hours for hexane to evaporate. The collection pot was filled with solutions of $AuCl_4^-$ at the required concentration, described in table 1.

Purification of particles

The collected sample was centrifuged (12000 rpm, 5 mins) and the supernatant discarded and reconstituted in acetonitrile (500 µL). The process was repeated with DI-water. The sample was then re-dispersed in DI-water (500 µL). When the sample contained iron oxide nanoparticles, the solution was placed next to a magnet (GE, healthcare, UK, Magrack) for 2 min. The supernatant was discarded, replaced with DI-water (100 µL) and sonicated for 1 min. This process was repeated three times with DI-water and twice with acetonitrile. The sample was then re-dispersed in either water or acetone (100 µL).

Electron microscopy

Scanning electron microscopy (SEM) samples were prepared by dropping the suspension onto conductive copper pad. A table top SEM Hitachi TM3030 was used for imaging particle sizes and distribution, and a FEG-SEM (FEG-SEM JEOL 7800F) was used for some higher resolution imaging of particles. Elemental composition of the particles was measured using the attached energy dispersive X-ray spectroscopy (EDS) to verify the chemistry of the particles. Transmission electron microscopy (TEM) specimens were prepared by ultrasonicating the suspensions followed by pipetting onto standard holey carbon film supported TEM grids (EM Resolutions Ltd, UK). A Jeol 2000FX TEM equipped with an Oxford Instruments (INCA350). The TEM was operated with 200kV accelerating voltage in conventional bright field mode. Selected area electron diffraction (SAED) patterns were recorded to identify the crystallinity of the particles.

Thickness of the Au nanoplates was measured by two methods: 1 electron energy loss spectroscopy (EELS) attached to a FEI Tecnai F20 G2 S-Twin field emission gun (FEG) TEM; 2 cross section SEM. The Tecnai F20 FEGTEM was operated at 200kV and equipped with a Gatan ENFINA EELS spectrometer. EELS is the analysis of the energy distribution of electrons that have come through the specimen including elastic scattered electrons (zero-loss

energy) and inelastic scatted electrons (low-loss and core-loss energy). The thickness of specimen can be determined by the equation $t/\lambda=\ln(I_t/I_0)$, where I_0 is the zero loss peak intensity, I_t is the total intensity in the low loss spectrum and λ is the average mean free path for these low energy losses, i.e. inelastic mean free path. The thickness can be worked out with an accuracy of ~±20% .

Powder X ray diffraction -
Samples were prepared for analysis by Powder X ray Diffraction (PXRD) from suspensions. The suspensions were dropped onto silicon substrates and the liquid allowed to evaporate before being placed into Perspex sample holders. The sample holders were loaded onto a Bruker D8 Avance Powder X ray Diffractometer set up in reflection geometry with Cu $K\alpha_1$ radiation (1.54056Å), selected from a Ge 111 monochromator and a LYNXEYE ™ 1D detector. Data were collected over the 2θ range 30-80° 2θ with a step size of 0.007° and a count time of 2 seconds per step.

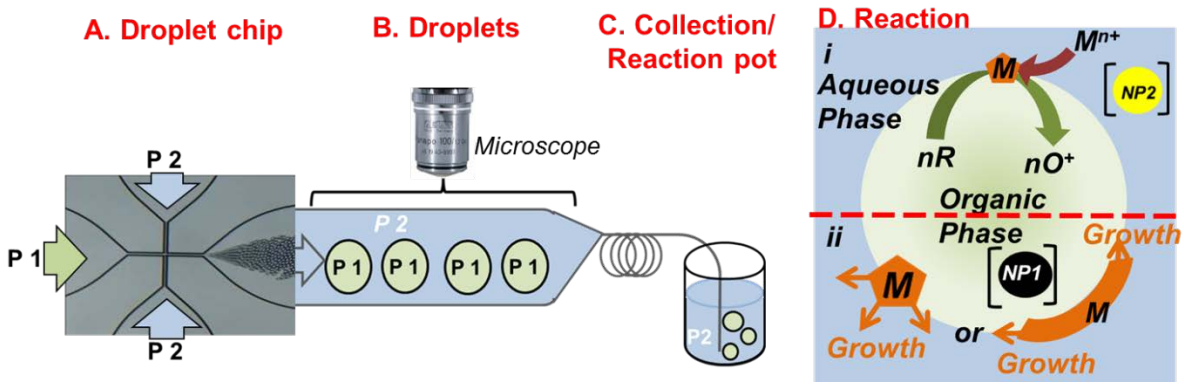

Figure 1 Schematic of the fluidic assembly and droplet collection. A) P1, P2 represents the organic and aqueous phase respectively. B) The chip allows the droplets to be imaged via an optical microscope. C) The droplets flowed through a tube approx. 5 cm long into a collection vial. D) i. Schematic of the reaction taking place at the liquid-liquid interface, n molecules of reductant, nR, are oxidised via the metal salt, M^{n+}, to create n moles of oxidised reagent, nO . ii. Product of the reaction adsorbed at the interface. Nanoparticle, NP1 or NP2 are presynthesised and dispersed in the organic or aqueous phase respectively.

Results and Discussion

Emulsion droplets were created within a microfluidic chip via a flow focusing strategy, a magnified section of the chip showing the droplet creation is given in Figure 1a. The droplet chip had a 14 μm restriction at its narrowest point. The full dimensions of the flow channels are given in supplementary Figure s1. The size of the droplets were controlled by the chip dimensions as well as the flow rate of the hexane (P1) and aqueous phase (P2). As the chips dimensions remain constant throughout the experiment, the droplet size is varied

by the relative flow rates of the liquids. Surfactant was initially required to stabilise the droplets, and SDS was selected as per previous work[61].

The droplet diameter that was created with this chip ranged from 5 to 30 μm. The size range was limited in part due to the chip dimensions, the low viscosity of the liquid and the flow rates that could be applied where the droplets could be clearly imaged on the microscope. The fluidic chip is optically transparent. This allowed a microscope coupled to a digital high resolution camera to image and size the droplets. Figure 1B shows schematic representation of data sets obtain and acquired images are given in Figure s2. The droplets then pass through a short tube into a collection pot. The elution time for the droplets was circa 1-2 mins, depending on the flow rates chosen, and upon entering the collection pot a magnetic stir bar was added in some experiments to aid their dispersion.

The concept is that, each droplet acts as a microreactor and this setup was recently used to assemble presynthesised AuNP on the surface of the hexane droplets[62]. The AuNPs were added to the aqueous phase, NP2 (Figure 1D) stabilising the droplets even in the absence of any other surfactant, i.e. a Pickering emulsion is formed. This process created a gold shell on top of iron oxide nanoparticles added to the hexane phase, NP1 (Figure 1D) creating core@shell particles. However, in this Pickering emulsion setup the gold shell was thin and nonuniform in its coverage. Thus, to advance their application herein, the hypothesis was to create and control the thickness of the gold shell, growing the gold particles through a chemical reaction, akin to growing a fresh layer of Au skin. A similar mechanism and process has been used with large free standing liq-liq interfaces creating a dense uniform layer of approximately 20 nm, spherical particles [42,45,63,64]. Here we adapt a reaction between tetrachloropalladate and DmFc[52], and a reaction scheme is shown in Figure 1D. As the newly formed droplets required a surfactant to stabilise them, a control experiment was performed to ascertain if Au particles can spontaneously form at a free standing Hexane/SDS/water interface. The resultant AuNPs are shown in Figure s3. TEM analysis shows that the particles observed via SEM are clusters of small approximately 70 nm AuNPs, Figure s3.

The same reaction was then performed at the interface of an emulsion droplet. To achieve this, the chip was filled until a steady stream of droplets were created, with both a DmFc hexane solution and an aqueous phase containing SDS. This was done to ensure no air bubbles are trapped in the device. Once a steady droplet stream had been created, e.g. Figure 1A, the aqueous solution was changed to include the $AuCl_4^-$ salt. Upon reinitiating the droplet stream it quickly became disrupted as the chip outlet became blocked or obstructed with debris, resulting in the droplets being trapped, coalescing and obstructing the flow of liquid. This observation was repeated several times on numerous chips and always resulted in a deposit on the chip surface that disrupted droplet production until it had been removed through washing with 5M HCl. Once the chip had been washed in HCl for several hours, it was able to be reused to produce droplets, but quickly became blocked again upon the addition of the $AuCl_4^-$ salt. It was assumed that the deposit was gold particles, and that the Au material was synthesised within seconds, causing the emulsion droplets to become unstable before exiting the chip. To avoid this problem, the droplets were first made in the presence of SDS before being dropped into the collection pot containing $AuCl_4^-$ as described in experiment B1, Table 1. The exit tube from the chip was always submerged at the bottom of the solution to aid dispersion and at least 5 ml of the $HAuCl_4$ solution was used. This was to

try and ensure the gold was always in excess, and the total volume of solvent used to make the emulsions was typically less than 1ml.

Table 1. Parameters for experiments liquid-liquid interface (B1,2). P1, P2 is the organic phase, and aqueous phase respectively.

Experiment	Classification	P1 (hexanes)	P2 (aqueous)	Reaction pot
B1	Au synthesis	DmFc (1-10 mM)	2%(wt/wt) SDS	$AuCl_4^-$ (5-10 mM)
B2	Au@Fe_3O_4 (CORE@SHELL)	DmFc (1-10 mM) 3mg/ml Ferrofluid	2%(wt/wt) SDS	$AuCl_4^-$ (5-10 mM)

During the reaction the collection pot changed from a yellow to green colour over a period of several minutes depending on the concentration of DmFc. After forming droplets for ~ 2 hours the pumps were switched off and the reaction pot was left for a minimum of 1 hour to allow the reaction to take place and hexane to evaporate. Following this the solution was centrifuged to collect the AuNP as described above.

Effects of droplet size; Figure 2a, shows an SEM image of the particles produced using droplets 22 μm ± 0.9 in diameter, with both the $AuCl_4^-$ and DmFc at 5 mM. Spherical particles were produced; although their size varied, it was typically much smaller than the initial droplet. Given that each DmFc molecule can only donate one electron, three mole equivalents of DmFc are required for each Au (III) ion. When placed in equivalent concentrations, the reaction would be limited by the DmFc. Keeping the concentration of the reactants the same and changing the droplet size should then result in different sized, or fewer, Au particles. The data shown in figure 2a-e are SEM images of Au particles produced for droplet sizes of 22 ± 0.9, 15 ± 0.76, 13 ± 1.6, 9 ± 1 and 7 ± 1 μm in diameter. The sizes of the spherical particles were 450 ± 124.1, 410 ± 128.1 and 250 ± 69.3 nm for droplet sizes of 22, 15 and 13 μm, respectively, as shown in Figures 2a-c. The data, including droplet and number of counted particles, are summarised in table s1, and we note that the concentrations of the particles were not measured. As the droplet diameter was decreased Au platelets were observed within the SEM images. This trend continued and as the droplet size was further reduced the number of platelets increased Figure 2f. The average size and number of each particle taken from multiple SEM images is given in table s1.

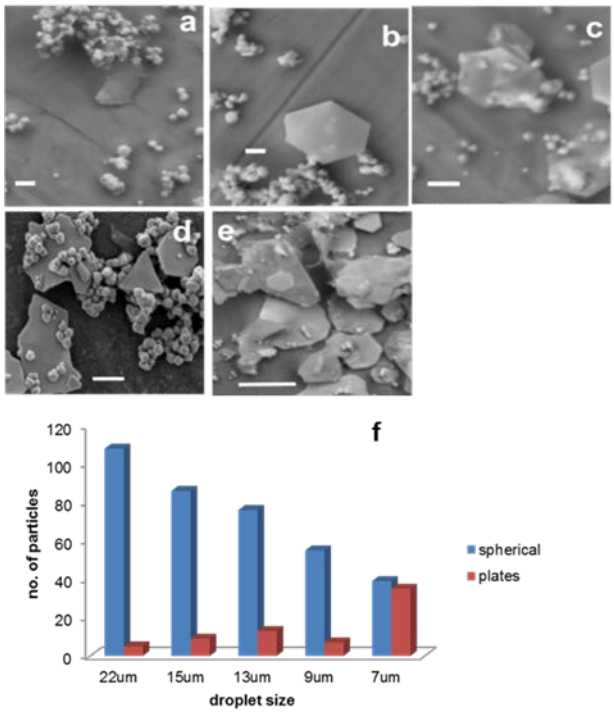

Figure 2 SEM of Au particle created under the conditions [$AuCl_4^-$] = 5 mM and [DmFc] = 5 mM. Droplet size a) 22 μm ± 0.9. b) 15.11μm ± 0.76 c) 13.4 μm ± 1.6 d) 9.1 μm ± 1 e) 7 μm ± 1. Scale Bar = 1 μm f) Graph that shows the effect of droplet size on the number of spheres and platelet particles, Blue – spheres and Red - platelets.

It was interesting and unexpected to see the appearance of gold platelets, and attempts were made to deduce the parameters that influenced their formation. The decrease in droplet size affects two parameters. First the total number of droplets created and secondly, the total surface area for the reaction to take place. The volume of hexane used to make the 22 and 7 micron droplets was similar: approximately 1 ml over 30 minutes. Therefore, as the volume remains constant, the number of droplets and the total surface area of all the droplets increases by approx. 31 and 3.1 times respectively, as the diameter decreases from 22 to 7 microns. Both factors may lead to a faster depletion of $AuCl_4^-$ around the droplets. To test the effects of $AuCl_4^-$ concentration on particle morphology two experiments were performed. The first was increasing the $AuCl_4^-$ concentration to 10 mM, and in a second experiment a stirrer bar was placed into the reaction pot to help further disperse the droplets. Neither of these had any effect on the number of platelets and the size of the spheres remained similar see Table s1, supplementary figure s4a-b. Lowering the $AuCl_4^-$ concentration to 1 mM resulted in the loss of the platelets, supplementary Figure s4c.

Effects of DmFc concentration; The size of the droplet was kept constant (circa 12 μm, approx. half way in the size range created in this setup), and the concentration of DmFc was then varied. As the concentration of DmFc was reduced from 10, 5 to 1 mM it was expected that the resultant spherical AuNP diameter would also decrease, given the total number of e^-

are reduced. The results are shown in Figures 3a-c, and tabulated in Table s1. In contrast, larger spherical particles were formed; in addition, the number of platelets also increased (figure 3b) leading to large Au platelets (>2 μm) as shown in Figure 3c. This may be due to the number of nucleation events decreasing as the concentration of DmFc is lowered, allowing fewer nuclei to grow to larger particles. The TEM images of the different shaped particles from Figure 3b are given in 3 d, e and the SAED pattern for the platelet is shown in Figure s5. The diffraction pattern shows the particles to be single crystals. The thickness of the platelets was also determined to be 36 ± 7 nm using EELS and cross-section SEM (see supplementary figure s6 and s7 respectively).

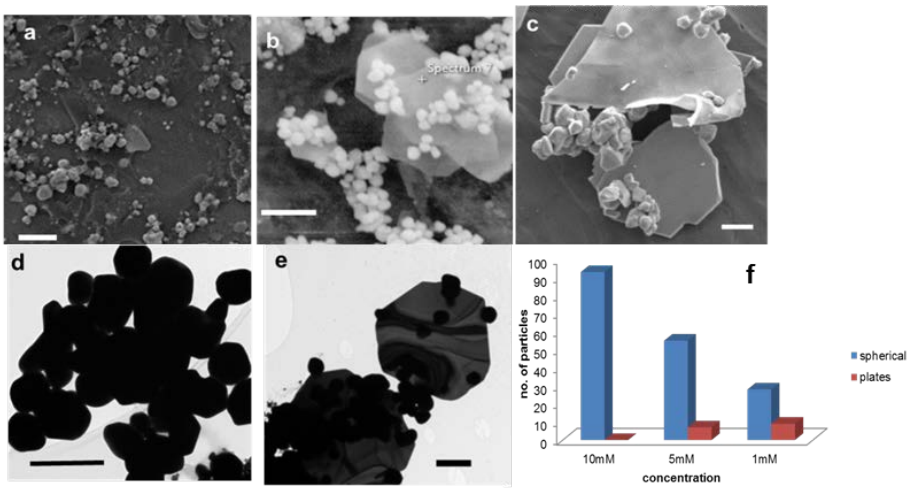

Figure 3 a) SEM image of Au particles, from a droplet size 11 μm ± 1.4, [$AuCl_4^-$] = 10 mM and [DmFc] = 10 mM, b) SEM image of Au, from a droplet size 10 μm ± 1, [$AuCl_4^-$] = 5 mM and [DmFc] = 5 mM. c) SEM image of Au particles, from a droplet size 12 μm ± 1, [$AuCl_4^-$] = 5 mM and [DmFc] = 1 mM. Scale bars 1 μm. d - e) TEM –of particles in figure b, scale bar 500 nm f) Graph that shows the effect of concentration of DmFc to the number of gold particles and platelets, Blue – spheres and Red – platelets.

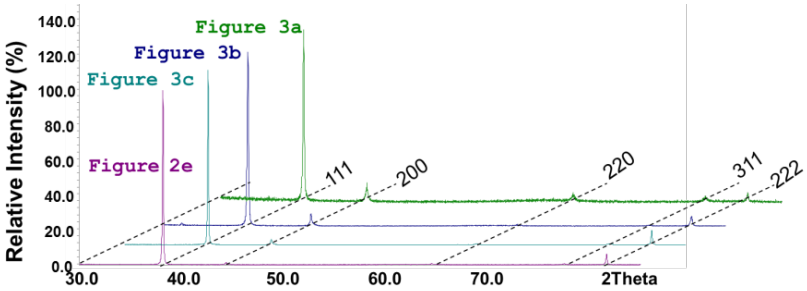

Figure 4 *XRD analysis of samples from figure 2 and 3, with offset to show the diffraction peaks.*

XRD analysis of the materials are shown in Figure 4. All the XRD data exhibit preferred orientation along the <111> direction, highlighted by the enhanced intensities of the 111 and 222 reflections. This is especially pronounced in the data shown for the samples in Figures 2e and 3c. As Au has a face centred cubic structure, this suggests its growth direction is along <111> which is common for face centred cubic materials and fits with the hexagonal platelet morphology, as observed in the SEM micrographs (Figures 2e and 3c respectively). The data from the sample corresponding to the micrograph in Figure 3a has greater peak widths, which suggests a smaller crystallite size and the peak shapes are also anisotropic, with a high angle tail (most pronounced for the reflection at 44.4° (2θ)). This could indicate the presence of different crystallite sizes, with sharper peaks superimposed on broader peaks. The SEM micrographs in Figures 3b and 3c suggest the presence of large platelets and smaller spherical particles, which correlate with the XRD data.

The sample in Figure 3b shows a mixture of spherical particles and platelets. The XRD data for this sample has a clear high angle asymmetry observed for the 200 reflection at 44.5° 2θ. Pattern fitting of these data allowed deconvolution of 2 peaks at this 2θ angle, with fitted Full Width Half Maxima (FWHM) of 0.1559 and 0.6525 ° 2θ. This would correspond to 2 crystallite sizes and it is suggested that the lower FWHM value is associated with the larger platelet morphology and hence the broader peak width is associated with the spherical particles. A similar observation can be made for the sample represented in Figure 3c, which is also a mixture of spherical particles and platelets and 2 peaks can be deconvoluted for the 200 reflection, with a sharp and broad FWHM; (0.1301 and 0.1693 respectively ° 2θ). The samples represented in Figures 3a and 2e have a broader FWHM for the 200 reflection, but less pronounced asymmetry and SEM confirms these samples have, predominantly, one morphology, a magnified view of the peak at 44.5° is given in supplementary Figure s8.

Mechanism; The growth of an Au particle across the interface as illustrated in Figure 1D would require an interfacial reaction. Both the metal, in P2, and reducing agent in P1 react at the interface to form the NP. It is however unclear if the nucleation of the particles takes place at the liq-liq interface, or as discussed elsewhere if the low solubility of the DmFc in water allows it to transfer to the aqueous phase before reacting to form nuclei[65]. Upon the formation of the nuclei it would then be energetically favourable for the nuclei to become adsorbed at the interface. Once fixed it can act as a conduit for electrons i.e. once created the particles growth could be autocatalytic as the electrons from the diffusing DmFc can be tunnelled across the metallic particle to a waiting $AuCl_4^-$ ion in the aqueous phase. DmFc has been shown to enhance electron transfer rates at AuNP functionalised liq-liq interfaces[66,67]. Such interfaces have also been shown to reduce O_2 forming H_2O_2, and the fermi level established across the interface is determined by the ratio of the $DmFc/DmFc^{+}$[66]. In this circumstance the nucleation of new particles may be slowed as the concentration of DmFc is depleted.

In the current setup the droplets are stabilised by SDS, and in some synthetic strategies SDS has been shown to produce asymmetric AuNPs[68,69]. In the examples here, we have a high throughput, room temperature synthesis strategy for producing platelets. To ascertain the influence of SDS on the particle morphology, it was removed and droplets were created and stabilised in the presence of small gold nanoparticles, NP2 (Figure 1D). These Pickering emulsions have been previously shown to form a gold layer on the outside of the droplets, stabilising the emulsion without the need for surfactant[62]. The AuNP's formed from the Pickering emulsion experiment are shown in Figure 5a. It is not clear if the Pickering particles acted as seeds to produce the cubic and platelet particles, and certainly not all of these initial Pickering particles are adsorbed into the growing phases as evident by their presence in the SEM. In the absence of the SDS, more cubic particles are produced as well as some platelets, which indicate that whilst SDS may play some role in templating the material it is not the only effect. Mixtures of CTAB and SDS were also used as alternative surfactants and the particles are shown in Figure 5b, and summarised in table s1. The platelets are no longer observed and only spherical particles remain. CTAB is known to have a strong influence on the growth of Au particles, although only spherical ones are observed here. Future work may allow the addition of specific surfactants to the reaction pot to produce a more uniform and controlled particle morphology. It is clear that whilst the surfactant has some influence on the resultant shape it is not be the only factor.

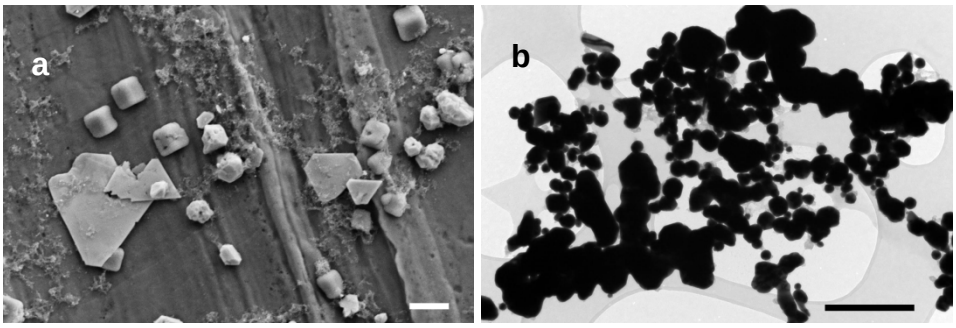

Figure5 a) SEM image of Au nanoparticles produced using pickering emulsions using droplet size 11.5 µm ± 2.2 [$AuCl_4^-$] = 5 mM and [DmFc] = 5 mM. Scale bar = 500 nm b) TEM image of Au nanoparticles using CTAB and SDS using droplet size 11.7 ± 1.8 [$AuCl_4^-$] = 5 mM and [DmFc] = 5 mM. Scale bar = 500 nm.

The growth of the NP will require the $AuCl_4^-$ salt to diffuse to the particles surface D1, and as DmFc is consumed by the growing particle its diffusion towards, D2, and away from the particle, D3. The electron transfer rate will also affect the particle growth. The mechanism for the production of Au platelets or spherical particles is determined by which process is the rate determining step, RDS. In most of the experiments we have the $AuCl_4^-$ at a high and consistent concentration; when it is lowered the particles tend towards a spherical morphology. The concentration of DmFc is a variable with a more pronounced effect on the shape. By lowering its concentration, more platelets are produced. Oxidation of the DmFc causes the fermi level, and electron transfer rate, across the interface to decrease. Thus for spherical particles a low concentration of $AuCl_4^-$ and high concentration of DmFc is required, and for platelets a high concentration of $AuCl_4^-$ and low DmFc concentration is preferred.

Interestingly if the concentration of the reactants remains constant and the droplets diameter decreased, data shown in Figure 2, the rapid conversion of the DmFc to $DmFc^+$ lowers the potential energy much faster and this slow growth leads to enlarged platelets.

Au@Fe_3O_4

Finally the setup was investigated to ascertain if core shell particles could be created. Fe_3O_4 nanoparticles were added to the hexane droplets with the DmFc. The resultant particles are shown in Figure 6a. As expected some platelets were produced alongside the more spherical particles, although the number of platelets were higher with the addition of the Fe_3O_4. As described above, we hypothesise that platelets are formed when the diffusion of the DmFc to the particle is the RDS. The addition of the Fe_3O_4 particles to the organic phase would act to slow the diffusion of the DmFc towards and away from the interface. In an attempt to reduce the number of platelets, the concentration of DmFc was increased to 50 mM and whilst this had the desired effect, some platelets are still visible, Figure 6b. All the particles imaged in Figure 6 were separated from solution and washed using a handheld magnet, and whilst not visible under the SEM the AuNPs must have either encapsulated or adsorbed some Fe_3O_4 particles on their surface. TEM analysis of the particles, Figure 6c, shows how each AuNP is surrounded by the Fe_3O_4 NPs, XRD data is given in Figure s9.

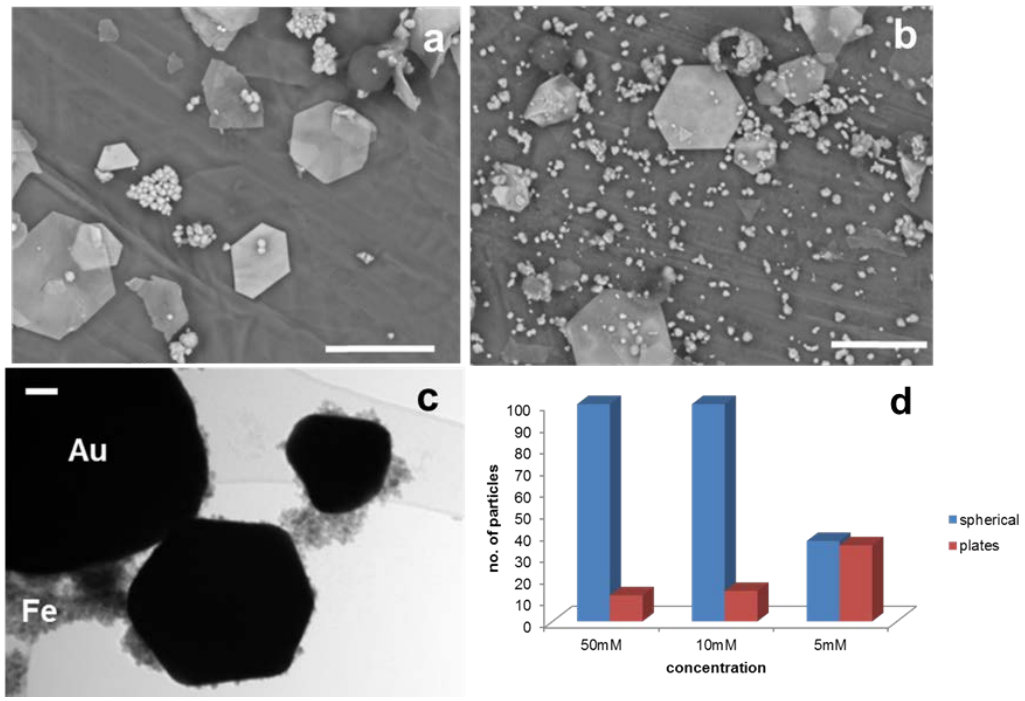

Figure 6 SEM Images of Au@Fe_3O_4 particles produced using a) Droplets size 11.3 μm ± 1.17 [$AuCl_4^-$] = 10 mM and [DmFc] = 5 mM. Scale bar = 5 μm. b) Droplets size 10.7 ± 0.81, [$AuCl_4^-$] = 10 mM and [DmFc] = 50 mM. Scale bar = 5 μm. c) TEM of particles produced droplets size 11.46 ± 1.4, [$AuCl_4^-$] = 10 mM and [DmFc] = 10 mM. Scale bar = 50 nm. d) Graph that shows the effect of the concentration of ferrofluid in DmFc

Conclusions

Here we present a method for synthesising and assembling nanomaterials at the liq-liq interface of an emulsion droplet. In an attempt to adorn each droplet with an Au nanoparticle skin, an interfacial reaction between decamethylferrocene (DmFc) in hexane and $AuCl_4^-$ within the aqueous phase, was employed to synthesise the Au nanoparticles on the droplets interface. In contrast to the same reaction at a large free standing interface which produces smaller spherical AuNPs, each droplet acted as a microreactor where the final size and shape of the NP was determined by the concentration of the DmFc or the size of the droplet. By tuning the reaction parameters either spherical single crystal AuNPs or single crystal micron sized Au platelets can be produced. We believe this could be a versatile platform for the large scale production of core@shell particles. The technique has the advantages of not requiring long reaction times, temperatures or templates to produce the asymmetric materials.

Acknowledgements

The work was supported by the European Commission for Research (PCIG11-GA-2012-321836 Nano4Bio). The authors acknowledge use of facilities within the Loughborough Materials Characterisation Centre

Conflicts of interest.

The authors declare no conflicts of interest

References

(1) Gou, L.; Murphy, C. J. Fine-Tuning the Shape of Gold Nanorods. *Chem. Mater.* **2005**, *17*, 3668–3672.
(2) Dreaden, E. C.; Alkilany, A. M.; Huang, X.; Murphy, C. J.; El-Sayed, M. A. The Golden Age: Gold Nanoparticles for Biomedicine. *Chem. Soc. Rev.* **2012**, *41*, 2740–2779.
(3) Lohse, S. E.; Murphy, C. J. The Quest for Shape Control: A History of Gold Nanorod Synthesis. *Chem. Mater.* **2013**, *25*, 1250–1261.
(4) Murphy, C. J. Biosensors: Plasmons Spring into Action. *Nat Mater* **2007**, *6*, 259–260.
(5) Peralta-Videa, J. R.; Zhao, L.; Lopez-Moreno, M. L.; de la Rosa, G.; Hong, J.; Gardea-Torresdey, J. L. Nanomaterials and the Environment: A Review for the Biennium 2008–2010. *J. Hazard. Mater.* **2011**, *186*, 1–15.
(6) Holzinger, M.; Le Goff, A.; Cosnier, S. Nanomaterials for Biosensing Applications: A Review. *Front. Chem.* **2014**, *2*, 63.
(7) Khot, L. R.; Sankaran, S.; Maja, J. M.; Ehsani, R.; Schuster, E. W. Applications of Nanomaterials in Agricultural Production and Crop Protection: A Review. *Crop Prot.* **2012**, *35*, 64–70.
(8) Rowland, C. E.; Brown III, C. W.; Delehanty, J. B.; Medintz, I. L. Nanomaterial-Based Sensors for the Detection of Biological Threat Agents. *Mater. Today*.
(9) Sajanlal, P. R.; Sreeprasad, T. S.; Samal, A. K.; Pradeep, T. *Anisotropic Nanomaterials: Structure, Growth, Assembly, and Functions*; 2011; Vol. 2.
(10) Salata, O. V. Applications of Nanoparticles in Biology and Medicine. *J. Nanobiotechnology* **2004**, *2*, 3.
(11) Stratakis, M.; Garcia, H. Catalysis by Supported Gold Nanoparticles: Beyond Aerobic Oxidative Processes. *Chem. Rev.* **2012**, *112*, 4469–4506.
(12) Mikami, Y.; Dhakshinamoorthy, A.; Alvaro, M.; Garcia, H. Catalytic Activity of Unsupported Gold Nanoparticles. *Catal. Sci. Technol.* **2013**, *3*, 58–69.
(13) Corma, A.; Garcia, H. Supported Gold Nanoparticles as Catalysts for Organic Reactions. *Chem. Soc. Rev.* **2008**, *37*, 2096–2126.
(14) Selvan, S. T.; Tan, T. T. Y.; Yi, D. K.; Jana, N. R. Functional and Multifunctional Nanoparticles for Bioimaging and Biosensing. *Langmuir* **2009**.
(15) Yu, C.; Irudayaraj, J. Multiplex Biosensor Using Gold Nanorods. *Anal. Chem.* **2006**, *79*, 572–579.
(16) Platt, M.; Willmott, G. R.; Lee, G. U. Resistive Pulse Sensing of Analyte-Induced Multicomponent Rod

Aggregation Using Tunable Pores. *Small* **2012**, *8*, 2436–2444.
(17) Storhoff, J. J.; Elghanian, R.; Mucic, R. C.; Mirkin, C. A.; Letsinger, R. L. One-Pot Colorimetric Differentiation of Polynucleotides with Single Base Imperfections Using Gold Nanoparticle Probes. *J. Am. Chem. Soc.* **1998**, *120*, 1959–1964.
(18) Liu, J.; Lu, Y. Preparation of Aptamer-Linked Gold Nanoparticle Purple Aggregates for Colorimetric Sensing of Analytes. *Nat. Protoc.* **2006**, *1*, 246–252.
(19) Liu, H.; Chen, D.; Li, L.; Liu, T.; Tan, L.; Wu, X.; Tang, F. Multifunctional Gold Nanoshells on Silica Nanorattles: A Platform for the Combination of Photothermal Therapy and Chemotherapy with Low Systemic Toxicity. *Angew. Chemie Int. Ed. 50*, 891–895.
(20) Bardhan, R.; Lal, S.; Joshi, A.; Halas, N. J. Theranostic Nanoshells: From Probe Design to Imaging and Treatment of Cancer. *Acc. Chem. Res.* **2011**, *44*, 936–946.
(21) Xu, X.; Zhao, Y.; Xue, X.; Huo, S.; Chen, F.; Zou, G.; Liang, X.-J. Seedless Synthesis of High Aspect Ratio Gold Nanorods with High Yield. *J. Mater. Chem. A* **2014**, *2*, 3528–3535.
(22) Tohidi, M.; Mahyari, F. A.; Safavi, A. A Seed-Less Method for Synthesis of Ultra-Thin Gold Nanosheets by Using a Deep Eutectic Solvent and Gum Arabic and Their Electrocatalytic Application. *RSC Adv.* **2015**, *5*, 32744–32754.
(23) Bullen, C.; Latter, M. J.; D'Alonzo, N. J.; Willis, G. J.; Raston, C. L. A Seedless Approach to Continuous Flow Synthesis of Gold Nanorods. *Chem. Commun.* **2011**, *47*, 4123–4125.
(24) Yeh, Y.-C.; Creran, B.; Rotello, V. M. Gold Nanoparticles: Preparation, Properties, and Applications in Bionanotechnology. *Nanoscale* **2012**, *4*, 1871–1880.
(25) Zeng, H.; Li, J.; Wang, Z. L.; Liu, J. P.; Sun, S. Bimagnetic Core/Shell FePt/Fe3O4 Nanoparticles. *Nano Lett.* **2004**, *4*, 187–190.
(26) Dosev, D.; Nichkova, M.; Dumas, R. K.; Gee, S. J.; Hammock, B. D.; Liu, K.; Kennedy, I. M. Magnetic/luminescent Core/shell Particles Synthesized by Spray Pyrolysis and Their Application in Immunoassays with Internal Standard. *Nanotechnology* **2007**, *18*, 55102.
(27) Amram, D.; Rabkin, E. Core(Fe)–Shell(Au) Nanoparticles Obtained from Thin Fe/Au Bilayers Employing Surface Segregation. *ACS Nano* **2014**, *8*, 10687–10693.
(28) Muehlethaler, C.; Leona, M.; Lombardi, J. R. Review of Surface Enhanced Raman Scattering Applications in Forensic Science. *Anal. Chem.* **2016**, *88*, 152–169.
(29) Edel, J. B.; Kornyshev, A. A.; Kucernak, A. R.; Urbakh, M. Fundamentals and Applications of Self-Assembled Plasmonic Nanoparticles at Interfaces. *Chem. Soc. Rev.* **2016**, *45*, 1581–1596.
(30) Edelstein, R. L.; Tamanaha, C. R.; Sheehan, P. E.; Miller, M. M.; Baselt, D. R.; Whitman, L. J.; Colton, R. J. The BARC Biosensor Applied to the Detection of Biological Warfare Agents. *Biosens. Bioelectron* **2000**, *14*, 805–813.
(31) Li, N.; Zhao, P.; Astruc, D. Anisotropic Gold Nanoparticles: Synthesis, Properties, Applications, and Toxicity. *Angew. Chemie Int. Ed.* **2014**, *53*, 1756–1789.
(32) Banu, K.; Shimura, T. Synthesis of Large-Scale Transparent Gold Nanosheets Sandwiched between Stabilizers at a Solid-Liquid Interface. *New J. Chem.* **2012**, *36*, 2112–2120.
(33) Duan, H.; Wang, D.; Li, Y. Green Chemistry for Nanoparticle Synthesis. *Chem. Soc. Rev.* **2015**, *44*, 5778–5792.
(34) Wiles, C.; Watts, P. Continuous Flow Reactors: A Perspective. *Green Chem.* **2012**, *14*, 38–54.
(35) Li, Y.; Sanampudi, A.; Raji Reddy, V.; Biswas, S.; Nandakumar, K.; Yemane, D.; Goettert, J.; Kumar, C. S. S. R. Size Evolution of Gold Nanoparticles in a Millifluidic Reactor. *ChemPhysChem* **2012**, *13*, 177–182.
(36) Okafor, O.; Weilhard, A.; Fernandes, J. A.; Karjalainen, E.; Goodridge, R.; Sans, V. Advanced Reactor Engineering with 3D Printing for the Continuous-Flow Synthesis of Silver Nanoparticles. *React. Chem. Eng.* **2017**.
(37) Ganguli, A. K.; Ganguly, A.; Vaidya, S. Microemulsion-Based Synthesis of Nanocrystalline Materials. *Chem. Soc. Rev.* **2010**, *39*, 474–485.
(38) Rahman, T. M.; Rebrov, V. E. Microreactors for Gold Nanoparticles Synthesis: From Faraday to Flow. *Processes* , 2014, *2*.
(39) Brust, M.; Walker, M.; Bethell, D.; Schiffrin, D. J.; Whyman, R. Synthesis of Thiol-Derivatised Gold Nanoparticles in a Two-Phase Liquid-Liquid System. *J. Chem. Soc. Chem. Commun.* **1994**, 801–802.
(40) Brust, M.; Fink, J.; Bethell, D.; Schiffrin, D. J.; Kiely, C. Synthesis and Reactions of Functionalised Gold Nanoparticles. *J. Chem. Soc. Chem. Commun.* **1995**, 1655–1656.
(41) Turkevich, J.; Stevenson, P. C.; Hillier, J. A Study of the Nucleation and Growth Processes in the Synthesis of Colloidal Gold. *Discuss. Faraday Soc.* **1951**, *11*, 55–75.
(42) Smirnov, E.; Scanlon, M. D.; Momotenko, D.; Vrubel, H.; Méndez, M. A.; Brevet, P.-F.; Girault, H. H. Gold Metal Liquid-Like Droplets. *ACS Nano* **2014**, *8*, 9471–9481.
(43) Fang, P.-P.; Chen, S.; Deng, H.; Scanlon, M. D.; Gumy, F.; Lee, H. J.; Momotenko, D.; Amstutz, V.;

Cortés-Salazar, F.; Pereira, C. M.; *et al.* Conductive Gold Nanoparticle Mirrors at Liquid/Liquid Interfaces. *ACS Nano* **2013**, *7*, 9241–9248.
(44) Grunder, Y.; Ramasse, Q. M.; Dryfe, R. A. W. A Facile Electrochemical Route to the Preparation of Uniform and Monoatomic Copper Shells for Gold Nanoparticles. *Phys. Chem. Chem. Phys.* **2015**, *17*, 5565–5568.
(45) Rao, C. N. R.; Kalyanikutty, K. P. The Liquid–Liquid Interface as a Medium To Generate Nanocrystalline Films of Inorganic Materials. *Acc. Chem. Res.* **2008**, *41*, 489–499.
(46) Ramsden, W. Separation of Solids in the Surface-Layers of Solutions and "Suspensions" (Observations on Surface-Membranes, Bubbles, Emulsions, and Mechanical Coagulation). -- Preliminary Account. *Proc. R. Soc. London* **1903**, *72*, 156–164.
(47) Pickering, S. U. CXCVI.-Emulsions. *J. Chem. Soc. Trans.* **1907**, *91*, 2001–2021.
(48) Platt, M.; Dryfe, R. A. W.; Roberts, E. P. L. Electrodeposition of Palladium Nanoparticles at the Liquid-Liquid Interface Using Porous Alumina Templates. *Electrochim. Acta* **2003**, *48*, 3037–3046.
(49) Platt, M.; Dryfe, R. A. W. Structural and Electrochemical Characterisation of Pt and Pd Nanoparticles Electrodeposited at the Liquid/liquid Interface: Part 2. *Phys. Chem. Chem. Phys.* **2005**, *7*, 1807–1814.
(50) Dryfe, R. A. W. Modifying the Liquid/liquid Interface: Pores, Particles and Deposition. *Phys. Chem. Chem. Phys.* **2006**, *8*, 1869–1883.
(51) Platt, M.; Dryfe, R. A. W.; Roberts, E. P. L. Controlled Deposition of Nanoparticles at the Liquid-Liquid Interface. *Chem. Commun.* **2002**, 2324–2325.
(52) Dryfe, R. A. W.; Simm, A. O.; Kralj, B. Electroless Deposition of Palladium at Bare and Templated Liquid/Liquid Interfaces. *J. Am. Chem. Soc.* **2003**, *125*, 13014–13015.
(53) Platt, M.; Dryfe, R. A. W.; Roberts, E. P. L. Structural and Electrochemical Characterisation of Pt and Pd Nanoparticles Electrodeposited at the Liquid/liquid Interface. *Electrochim. Acta* **2004**, *49*, 3937–3945.
(54) Booth, S. G.; Dryfe, R. A. W. Assembly of Nanoscale Objects at the Liquid/Liquid Interface. *J. Phys. Chem. C* **2015**, *119*, 23295–23309.
(55) Banu, K.; Shimura, T. Synthesis of Large-Scale Transparent Gold Nanosheets Sandwiched between Stabilizers at a Solid-Liquid Interface. *New J. Chem.* **2012**, *36*, 2112–2120.
(56) Reymond, F.; Fermín, D.; Lee, H. J.; Girault, H. H. Electrochemistry at Liquid/liquid Interfaces: Methodology and Potential Applications. *Electrochim. Acta* **2000**, *45*, 2647–2662.
(57) Girault, H. Electrochemistry at Liquid/Liquid Interfaces. In *Electroanalytical Chemistry*; Electroanalytical Chemistry: A Series of Advances; CRC Press, 2010; pp. 1–104.
(58) Schaming, D.; Hojeij, M.; Younan, N.; Nagatani, H.; Lee, H. J.; Girault, H. H. Photocurrents at Polarized Liquid|liquid Interfaces Enhanced by a Gold Nanoparticle Film. *Phys. Chem. Chem. Phys.* **2011**, *13*, 17704–17711.
(59) Lee, K. Y.; Kim, M.; Han, S. W. Controlled Synthesis of Au Nanoplates at the Liquid/liquid Interface. *Mater. Lett.* **2009**, *63*, 480–482.
(60) Rodgers, A. N. J.; Booth, S. G.; Dryfe, R. A. W. Particle Deposition and Catalysis at the Interface between Two Immiscible Electrolyte Solutions (ITIES): A Mini-Review. *Electrochem. commun.* **2014**, *47*, 17–20.
(61) O'Mahony, J. J.; Platt, M.; Kilinc, D.; Lee, G. Synthesis of Superparamagnetic Particles with Tunable Morphologies: The Role of Nanoparticle-Nanoparticle Interactions. *Langmuir* **2013**, *29*, 2546–2553.
(62) Sachdev, S.; Maugi, R.; Kirk, C.; Zhou, Z.; Christie, S. D. R.; Platt, M. Synthesis and Assembly of Gold and Iron Oxide Particles Within an Emulsion Droplet; Facile Production of Core@Shell Particles. *Colloid Interface Sci. Commun.* **2017**, *16*, 14–18.
(63) Booth, S. G.; Uehara, A.; Chang, S. Y.; Mosselmans, J. F. W.; Schroeder, S. L. M.; Dryfe, R. A. W. Gold Deposition at a Free-Standing Liquid/Liquid Interface: Evidence for the Formation of Au(I) by Microfocus X-Ray Spectroscopy (μXRF and μXAFS) and Cyclic Voltammetry. *J. Phys. Chem. C* **2015**, *119*, 16785–16792.
(64) Luo, K.; Schroeder, S. L. M.; Dryfe, R. A. W. Formation of Gold Nanocrystalline Films at the Liquid/Liquid Interface: Comparison of Direct Interfacial Reaction and Interfacial Assembly. *Chem. Mater.* **2009**, *21*, 4172–4183.
(65) Su, B.; Hatay, I.; Li, F.; Partovi-Nia, R.; Méndez, M. A.; Samec, Z.; Ersoz, M.; Girault, H. H. Oxygen Reduction by Decamethylferrocene at Liquid/liquid Interfaces Catalyzed by Dodecylaniline. *J. Electroanal. Chem.* **2010**, *639*, 102–108.
(66) Scanlon, M. D.; Peljo, P.; Mendez, M. A.; Smirnov, E.; Girault, H. H. Charging and Discharging at the Nanoscale: Fermi Level Equilibration of Metallic Nanoparticles. *Chem. Sci.* **2015**, *6*, 2705–2720.
(67) Peljo, P.; Manzanares, J. A.; Girault, H. H. Contact Potentials, Fermi Level Equilibration, and Surface Charging. *Langmuir* **2016**, *32*, 5765–5775.
(68) Moon, S. Y.; Kusunose, T.; Sekino, T. CTAB-Assisted Synthesis of Size- and Shape-Controlled Gold

Nanoparticles in SDS Aqueous Solution. *Mater. Lett.* **2009**, *63*, 2038–2040.
(69) Kuo, C.-H.; Chiang, T.-F.; Chen, L.-J.; Huang, M. H. Synthesis of Highly Faceted Pentagonal- and Hexagonal-Shaped Gold Nanoparticles with Controlled Sizes by Sodium Dodecyl Sulfate. *Langmuir* **2004**, *20*, 7820–7824.

TOC